

## THE NEED FOR CONTROL EXPERIMENTS IN LOCAL HELIOSEISMOLOGY

Joseph Werne<sup>1</sup>, Aaron Birch<sup>1</sup>, and Keith Julien<sup>2</sup>

<sup>1</sup>*CoRA Division, NorthWest Research Associates, 3380 Mitchell Lane, Boulder, CO 80301, USA,  
werne@cora.nwra.com, aaronb@cora.nwra.com*

<sup>2</sup>*Department of Applied Mathematics, University of Colorado, Campus Box 526, Boulder, CO 80309, USA,  
julien@colorado.edu*

### ABSTRACT

The key to local helioseismology is the effective application of local seismic diagnostic techniques to determine the structure of the solar interior with the finest possible resolution. The extent and magnitude of the supergranular return flow and the nature of thermal anomalies, flows, and magnetic-field configurations in and near active regions are phenomena on which we hope local helioseismic analyses will shed clear light. However, current applications of local seismic methods produce ambiguous and inconsistent interpretations. It is clear that in order to make further progress, evaluation and refinement of local analysis techniques, and the development of procedures that can separate magnetic effects, subsurface flows, and sound-speed variations will prove critical. We believe substantial progress in this area can be made by conducting control experiments based on magneto-acoustic-gravity waves propagating through specified models of subphotospheric anomalies. In this paper we describe the need for such an effort and developments currently under way to produce the tools necessary to implement a validation and testing program.

Key words: local helioseismology; synthetic data.

### 1. INTRODUCTION

A great deal of our present knowledge of solar-interior structure and dynamics developed during the 1970s and 1980s via the application of *global helioseismology*, i.e., the identification of global modes of solar oscillation and accurate measurements of their frequencies (Christensen-Dalsgaard 2002). The recognition of *local helioseismology* as a major new field of solar research has grown mostly since the late 1980s, with the advent of high-spatial-resolution helioseismic observations of the solar surface.

Today, techniques in local helioseismology are providing us with subphotospheric maps of the supergranulation and of flow patterns and sound-speed variations surrounding active regions. Local diagnostics are showing us large-scale azimuthal and meridional flows and monitoring active regions on the Sun's far surface. Local diagnostics promise detailed physical models of thermal features and flows ranging from the surface to deep within the solar interior.

Despite the considerable progress, various artifacts and biases have been identified as causes for concern in local analysis, including large distortions of the amplitude and phase of the wave field due to surface magnetic fields (Lindsey & Braun 2003, 2004b) and the effects of wave absorption in sunspots and plages (Woodard 1997, Gizon & Birch 2002). Strong localized absorption of waves may contribute to acoustic signatures that mimic zones of convergence around active regions obtained from ring diagram analysis (Haber et al. 2002). In addition, Braun & Lindsey (2003) argue that the signature of an apparent supergranular return flow 10 Mm beneath the photosphere is largely an artifact of the surface-flow pattern.

As a result of these and other uncertainties, seemingly disparate conclusions have been drawn about the nature of subsurface structure and dynamics. As a case in point, consider the divergent values reported for the depth of supergranular flows. Braun & Lindsey (2003) estimate the depth of the supergranular return flow to be 3 Mm or less, while Duvall (1998) estimates the same at 5–8 Mm, and Zhao & Kosovichev (2002) estimate it at 15 Mm. The estimates from the latter two studies are based on the vertical correlation of the inferred horizontal velocity field (or its derivatives) to deduce evidence of a return flow, while Braun & Lindsey (2003) examine the vertical correlation of (unmodeled) phase-sensitive holography signatures at different focus depths. They suggest the observations are consistent with near-surface flow only. They caution that a straightforward seismic interpretation at a substan-

tial depth is confounded by the nature of the supergranular surface-flow pattern combined with details of the local seismic analysis methods being used (Braun & Lindsey 2003). Subsequent work incorporating forward modeling based on specified supergranular flow patterns confirms their concerns and indicates that our knowledge of flow on supergranular scales becomes increasingly murky below 3 Mm below the surface (Braun et al. 2004).

Another phenomenon yielding alternate and seemingly conflicting inferences involves sound-speed variations and flows beneath and around active regions. For example, with regard to sound-speed variations, measurements by Kosovichev et al. (2000) indicate sound speeds up to 1 km/s less than in the quiet subphotosphere from the surface down to about 3 Mm, and up to 1 km/s greater at depths between 3 and 10 Mm. In contrast, relatively superficial (i.e. less than a few Mm deep) sound-speed perturbations in active regions are suggested by other models of local helioseismic observations (Fan, Braun & Chou 1995, Braun & Lindsey 2000, Lindsey & Braun 2003, 2004a, Cally et al. 2003). Similarly, with regard to flows, Duvall et al. (1996) infer outflows around and downflows beneath sunspots. They interpret the outflows as relatively shallow and speculate on the existence of deeper inflows to feed the downflows. Lindsey et al. (1996), using spectral masks for “knife-edge” imaging, also infer outflows, but their measurements suggest the outflows persist with depth and evolve rapidly as the active region matures. Subsequent work by Braun (1997) presents evidence suggesting observed travel-time asymmetries in sunspots are not consistent with flows. Later work by Braun & Lindsey (2000, 2003) continues to stress near-surface (i.e.,  $0 < z < 3$  Mm) outflows, but expresses concern over surface artifacts which might confuse deeper analysis. In contrast, Zhao et al. (2001) and Zhao & Kosovichev (2003) report powerful inflows and associated downflows from 1.5–5 Mm and strong outflows beneath, which extend laterally outward to more than 30 Mm. Very recent work examining the phase of holographic “control-correlations” by Lindsey & Braun (2004a) reports asymmetries analogous to those previously observed by Braun (1997).

Given the basic, qualitative differences in the reported seismic results for active regions, readers should welcome the cautionary comments offered by most authors working in this area. To cite a few examples of authors’ concerns regarding their own work, we begin with Zhao et al. (2001), who comment, “We assume the travel-time differences are completely due to mass flows. Woodard (1997) and Birch & Kosovichev (2000) argue that some other factors, such as nonuniform distributions of acoustic sources and finite-wavelength effects may also affect travel times, which may greatly complicate our analysis and in particular our quantitative inferences.” Similarly, Lindsey et al. (1996) remark that “it is possible that the horizontal Doppler diagnostic is

sensitive to other processes besides horizontal flows and these could invalidate our interpretation in terms of submerged outflows.” Indeed, when contemplating the seemingly inconsistent mass-flow configuration reported by Lindsey et al. (1996), which they themselves refer to as “quite complex if not a little diabolical,” one senses an urgent need to examine alternative processes that could explain the reported seismic signatures. As Lindsey et al. (1996) stress, “it is important that we carefully examine processes other than subsurface flows that could give rise to the features we are seeing.” An obvious candidate for a potentially confounding effect near and around sunspots is the influence of magnetic fields on magneto-acoustic-wave propagation (e.g., Lindsey & Braun 2004a,b); nevertheless, systematic application of procedures to infer magnetic-field configurations separate from coincident subsurface flows has yet to be attempted.

Clearly, synthetic seismic test-data sets based on 3-D spatial data volumes which specify various flow and magnetic-field configurations would be immensely valuable for evaluating and refining current methods for determining flows near and beneath active regions. Numerically simulated magneto-acoustic-gravity (MAG) waves generated by specified sources and propagating through specified subsurface perturbation fields would help us establish meaningful uncertainties in seismic diagnostic procedures. Control studies based on known thermal, magnetic, and flow-field perturbations would help us separate our understanding of the subsurface solar phenomenon being studied from the seismic methods being employed. In this regard we agree with researchers who stress the need for validation tests incorporating artificially generated data sets, e.g.:

“We believe that future studies using synthetic data calculated by finite-difference modeling, possibly including flows and magnetic fields, will improve our understanding of both time-distance data and the obtained inversion results.”  
–Jensen et al. (2003)

“In our opinion, credible simulated sound computations have become the crux of a clear understanding of the subphotospheres of active regions.”  
–Lindsey & Braun (2004b)

“Understanding absorption and scattering [by magnetic fields] will be necessary if time-distance studies are to be placed on a firm theoretical footing.”  
–Rosenthal & Julien (2000)

“The analysis of artificial data produced via large-scale convection simulations will surely aid in our understanding of various

approaches to time-distance analysis.”  
–Birch (2004)

“Validating time-distance helioseismology with realistic numerical simulations will be one of the most exciting things to come in the next 5 years.”  
–Gizon (2004)

It is our goal to help establish a program with which this clear need for artificial data for local helioseismic testing will be filled. In such a program, we feel it is necessary to consider the various approximations and simplifying assumptions on which different seismic diagnostic techniques depend and systematically evaluate the impact of these assumptions on the results obtained. As such, we think the establishment of standard test-data sets for simultaneous interrogation by multiple local seismic approaches is important. A critical component of a validation and testing effort will be a flexible facility for creating artificial data specifically designed to address individual questions for which answers are currently ambiguous.

### 1.1. Previous tests with artificial wavefield computations

Preliminary efforts have already begun to produce and interpret local helioseismic signatures using artificial seismic data. Julien et al. (1995), for example, evaluated the feasibility of an inversion procedure using Hilbert transforms to deduce subsurface sound-speed variations. They found that spurious signals resulting from mode beating between nearly parallel monochromatic waves contaminated the inversion. These signals possess zero group velocity and therefore could not be swept out of the target domain as hoped by Gough et al. (1992) who solved the equivalent 1-D problem. Birch et al. (2001) carried out a single-source/single-receiver experiment via time-distance correlations of waves passing through spherically symmetric perturbations in a homogeneous medium. They compared results from finite-difference wave-propagation simulations with time-distance methods based on the ray and Born approximations so that they could evaluate the accuracy of these methods. Skartlien (2002) also employed single-source/single-scatterer as well as multiple-source/single-scatterer experiments for demonstrating an inversion technique for holographic signatures. These approaches indicate the utility of direct simulations to generate and use artificial seismic data to evaluate local helioseismic analysis methods applied to subsurface thermal anomalies.

Others who employed single-source acoustic-propagation simulations include Barnes & Cally (2001) and Tong et al. (2003a,b). Barnes & Cally (2001) simulated 2-D acoustic waves that propagate from a compact source oscillating at multiple distinct frequencies in a hydrostatic polytropic background.

They demonstrated the degradation in resolving ability that results when holographic methods neglect wave dispersion. They then computed more accurate ray paths appropriate for polytropic and more realistic solar models that could be used in dispersive environments. Tong et al. (2003a,b) similarly used acoustic propagation simulations to examine errors introduced by dispersive effects. Based on their results they advocate the use of wave-field tomographic methods in order to enhance spatial resolution beyond that currently achieved with current time-distance methods (Tong et al. 2003a,b).

Simulations designed to elucidate the coupling between magnetic fields and acoustic waves in active regions are currently being conducted by Paul Cally and colleagues (Cally & Bogdan 1997, Cally 2000, Cally et al. 2003, and Cally 2004). Their work and that of Rosenthal & Julien (2000) has examined the evolution of  $f$  and  $p$  modes as they interact with simple magnetic structures in a vertically stratified 2-D (or 2.5-D, in the case of Rosenthal & Julien 2000) medium. Results have been used to interpret measurements of absorption and scattering in sunspots (Braun 1995), and they reported the relative strength of acoustic- and Alfvén-wave coupling and apparent  $p$ -mode absorption as a function of depth and magnetic-field configuration in the solar interior. The computed results demonstrate the need to develop local seismic techniques for distinguishing magnetic-field/acoustic-wave interactions from subsurface flows. Artificial data sets based on simulations like these could serve as a test-bed for developing such algorithms. The time steps and spatial resolutions required by these studies indicate that full 3-D MAG-wave simulations are quite feasible.

Finally, Jensen et al. (2003) were the first to perform fully 3-D acoustic propagation simulations to test local helioseismic methods. Their finite-difference calculations covered a  $160 \text{ Mm} \times 160 \text{ Mm} \times 75 \text{ Mm}$  volume of the solar interior just below the photosphere. They used sound-speed and density profiles from model  $S$  of Christensen-Dalsgaard et al. (1996), and they added a thermal anomaly intended to model the sound-speed deficit associated with a 20 Mm diameter sunspot extending from the surface to a depth of 30 Mm; see Figure 1. The sound-speed structure they chose is based on observations modeled by Kosovichev et al. (2000).

The anomaly was illuminated by acoustic radiation from a layer of random-strength sources 500 km below the domain surface. The time history each source was a Ricker wavelet (2nd derivative of a Gaussian), which is band limited with a central frequency of  $\nu = 3.15 \text{ mHz}$  and a FWHM frequency range of  $\Delta\nu = 3.64 \text{ mHz}$ . Synthetic 8-hr Dopplergrams were constructed by sampling the upper-boundary free-surface motion with a spatial and temporal resolution consistent with MDI high-resolution data.

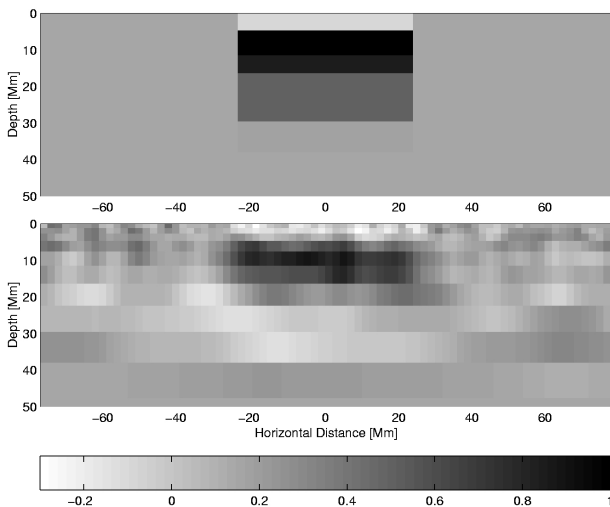


Figure 1. Inversion of simulated acoustic wavefield from Jensen et al. (2003). Top panel shows a cross section of the model sound-speed perturbation. Bottom panel shows the reconstructed sound-speed perturbation from an inversion of simulated acoustic waves propagated through the model. Color bar shows the sound-speed scale in km/s.

Inversion results computed by Jensen et al. (2003) are shown in Figure 1. Some important aspects of the anomaly are recovered by the inversion, such as the sound-speed decrease near the surface and the sound-speed maximum below, but deeper properties are only faintly represented. Jensen et al. (2003) noted that the recovered sound-speed variation is at best only a noisy representation of the specified anomaly as a result of estimation error associated with the limited duration over which cross-correlations were computed. By comparing regions remote from and within the anomaly in the upper and lower panels of Figure 1, we can gage the signal-to-noise ratio  $r$  of the reconstructed field to be  $r = 1.0$  to  $2.5$  above  $z = 10$  Mm and  $r < 1.0$  at greater depth. Also, the spatial resolution appears to be 2–5 Mm above  $z = 10$  Mm, and coarser below. This is consistent with an  $O(\lambda)$  resolution limit, noting that for solar model  $S$ , the sound-speed variation is such that  $\nu = 3.15$  mHz corresponds to acoustic wavelengths  $\lambda$  which vary smoothly from  $\lambda \approx 7.3$  Mm at a depth of  $z = 5$  Mm to  $\lambda \approx 22.5$  Mm at  $z = 30$  Mm. These resolution and signal-to-noise characteristics agree well with theoretical discussions in Gizon & Birch (2004).

It is important to point out the fundamental difference between the artificial-seismic-data studies discussed in this section and more conventional forward-modeling approaches which do not employ wave-propagation simulations (e.g., Kosovichev & Duvall 1997, Korzennik 2001, Zhao et al. 2001). Instead, these studies prepare artificial data using the same sensitivity kernels employed to perform the inversion. In many cases, no noise is added when solving the for-

ward problem, so that very clean and uniformly well-resolved test inversions result (e.g., see Kosovichev & Duvall 1997 and Zhao et al. 2001). Though limitations are indeed uncovered by these methods (e.g., the inability to accurately determine vertical flows at depths where the phase velocity of the illuminating waves is predominantly horizontal), the impact of finite-time sampling error and depth-dependent-resolution limits are masked by these noise-free procedures. Korzennik (2001) took steps to address these effects by adding varying amounts of white noise to his travel-time differences before inverting his test data. Useful results are obtained demonstrating the impact noise has on resolving ability. Nevertheless, white noise does not contain the spatial and temporal correlations in real data which result from MAG waves propagating from localized sources. Furthermore, by directly simulating the coupling between Alfvén and acoustic waves, the acoustic absorption and phase shifts due to magnetic fields can be directly evaluated and need not be modeled. In order to address these and other effects, the use of wave-propagation simulations to generate synthetic seismic signals is essential.

## 2. TESTING PROGRAM FOR LOCAL HELIOSEISMOLOGY

It is our opinion that the work described above demonstrates the feasibility of full 3-D wave-propagation simulations for generating synthetic seismic data for local-helioseismology testing and validation. As such, with some coordinated effort, we sense that a comprehensive local-helioseismology testing program based on artificial data is realizable. The pioneering work of Jensen et al. (2003) represents a pivotal step. Though at this point they have only examined thermal perturbations of the background solar model, the test-bed framework they have constructed is a model for future work. Adding subphotospheric ingredients, like flows and magnetic fields, and improving the accuracy of numerical boundary treatments will extend the utility of the artificial data generated. A testing program based on improved synthetic seismic data would help answer important open questions, such as: 1) How does the character of solar sound sources impact the resolving ability of local helioseismology methods? 2) What signatures does acoustic-wave damping project into the various seismic diagnostics currently being used? 3) How can the effects of magnetic fields be clearly distinguished from those of flows? 4) How can we quantify the impact of the “acoustic showerglass” discussed by Lindsey & Braun (2004b)? Can analysis algorithms be developed that mitigate its seismic effects? And 5) what are the inherent limitations of the various seismic analysis methods? These questions are ripe for examination via control experiments using artificial-data techniques, and some cannot be efficiently answered by other means.

We have begun putting the pieces in place to help establish the code needed to generate artificial test-data sets. It is our intention to make standard test-data sets available so that multiple local helioseismology methods (e.g., time-distance, acoustic holography, ring diagrams, etc.) can be applied. In the remainder of this paper we describe the necessary components to build the needed wave-propagation code(s), which include 1. solving the equations of motion for MAG-wave propagation (§2.1), 2. refining boundary treatments so that simulated waves may freely propagate out of the numerical domain (§2.2), 3. specifying sound sources (§2.3), and 4. numerical implementation of the above (§2.4). §3 presents a simple example involving photospheric flows.

## 2.1. Model equations for wave simulation

Throughout most of the solar interior, wave amplitudes  $v$  are significantly less than the sound speed  $c$  (i.e.,  $v/c \lesssim 0.04$  and rapidly decreasing with depth). Therefore, the nonlinear terms that describe the mutual interaction of waves can be safely neglected throughout most of the solar interior. An important exception is the uppermost layers of convection near the photosphere where turbulent motion, intense thermal plumes, and localized shocks can excite the seismic waves helioseismology seeks to diagnose. We will model this wave-generation process; see §2.3. Hence, with sound sources specified, the relevant equations of motion for wave-propagation studies are the linear compressible MHD equations:

$$\rho_0 \left( \frac{\partial \mathbf{u}}{\partial t} + \mathbf{U}_0 \cdot \nabla \mathbf{u} + \mathbf{u} \cdot \nabla \mathbf{U}_0 \right) + \rho \frac{\partial \mathbf{U}_0}{\partial t} = -\nabla p - \rho g \hat{\mathbf{z}} + \frac{1}{4\pi} [(\nabla \times \mathbf{B}_0) \times \mathbf{b} + (\nabla \times \mathbf{b}) \times \mathbf{B}_0] + \mathbf{S} \quad (1)$$

$$\frac{\partial \rho}{\partial t} + \nabla \cdot (\rho_0 \mathbf{u} + \rho \mathbf{U}_0) = 0 \quad (2)$$

$$\frac{\partial p}{\partial t} + \mathbf{U}_0 \cdot \nabla p + \mathbf{u} \cdot \nabla P_0 = -c^2 (\rho_0 \nabla \cdot \mathbf{u} + \rho \nabla \cdot \mathbf{U}_0) + S_p \quad (3)$$

$$\frac{\partial \mathbf{b}}{\partial t} = \nabla \times (\mathbf{U}_0 \times \mathbf{b} + \mathbf{u} \times \mathbf{B}_0) + \mathbf{S}_b \quad (4)$$

$$\nabla \cdot \mathbf{b} = 0 \quad (5)$$

Here  $p(\mathbf{x}, t)$ ,  $\rho(\mathbf{x}, t)$ ,  $\mathbf{u}(\mathbf{x}, t)$ , and  $\mathbf{b}(\mathbf{x}, t)$  are the spatially and temporally varying pressure, density, velocity and magnetic disturbances associated with the wave field, and  $P_0(\mathbf{x}, t)$ ,  $\rho_0(\mathbf{x}, t)$ ,  $\mathbf{U}_0(\mathbf{x}, t)$ , and  $\mathbf{B}_0(\mathbf{x}, t)$  specify the subsurface anomaly and base-state profiles.  $c^2 = \gamma P_0 / \rho_0$  is the squared sound speed;  $\gamma$  is the ratio of specific heats.  $\mathbf{S}$ ,  $S_p$ , and  $\mathbf{S}_b$  represent nonlinear wave-source, radiative damping, and magnetic resistivity terms.

Advantages to solving the linearized MHD equations include:

1. Because interactions between waves are absent, truncation of the wave spectrum to a specified wavenumber band is permitted. This can greatly reduce the computational memory requirements compared to fully nonlinear simulations which must either resolve or model the smallest scales of motion.
2. Aliasing errors (Canuto et al. 1988) encountered when evolving linear waves are not as severe as for fully nonlinear systems. Coupling between the wave and anomaly fields can be evaluated beforehand so that only the minimum necessary truncation may be performed when de-aliasing the computed solutions.
3. Because linear solutions to the compressible MHD equations do not steepen into shocks, higher-order numerical methods (e.g., pseudo-spectral methods), which require smooth solutions can be employed. This promises much greater spatial resolution and much smaller dispersion errors for MAG-wave simulations than is possible with finite-difference approaches.
4. Highly accurate wave-transmission boundary conditions can be developed for linear waves.
5. Because nonlinear-source, radiation, and damping terms are independently specified using the variables  $\mathbf{S}$ ,  $S_p$ , and  $\mathbf{S}_b$ , distinct control experiments can be designed to address specific questions related to local helioseismology analysis.

These advantages offer us the flexibility to separately specify and therefore individually examine the impacts of different physical effects, such as sound-source distribution and temporal spectra, varied radiation treatments, and turbulent diffusion and turbulent magnetic resistivity. The linear framework also allows us to separately study thermal, flow, and magnetic anomalies as well as their varied combinations. As such, solutions to these equations offer an ideal facility for systematically conducting needed local helioseismology control experiments.

## 2.2. Boundary conditions

It is important that the specified boundary conditions accurately represent the interior medium in response to incident waves. This means the upper boundary should annihilate waves that should not be reflected back into the solar interior below the middle chromosphere, i.e., those with frequency  $\nu$  above the acoustic cutoff  $\nu > \nu_c$ . Similarly, side and bottom boundaries must be able to dispose of waves as though transmitted freely through the boundary without reflection. This will insure the domain does not become an unintended acoustic cavity. In addition, we must be able to specify waves which propagate into the domain from the outside.

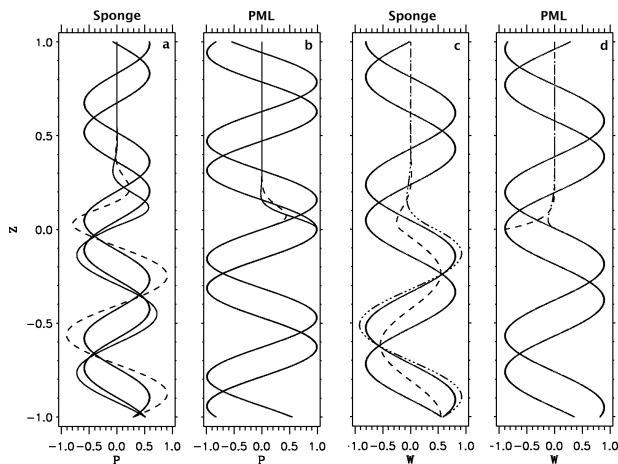


Figure 2. Computed real (dashed) and imaginary (dot-dashed) components of a wave forced at the bottom of a domain employing various wave reflection conditions at  $z = 0$ . Thick solid curves indicate the exact solutions for the real and imaginary parts. a) Sponge layer for an acoustic wave; b) PML for an acoustic wave; c) Sponge layer for a gravity wave; d) PML for a gravity wave. The PML conditions produce solutions outside the damping layer (i.e.,  $z < 0$ ) which are indistinguishable from the exact solution, while the sponge-layer conditions reflect wave energy back into the domain where it becomes trapped and contaminates the solution.

One might attempt to handle these issues on the side boundaries by using periodic conditions and domains which are significantly wider than the typical damping length  $\ell_d \approx 30$  Mm for solar acoustic waves. This approach, however, will increase the memory and cost required for the simulation, perhaps unnecessarily. And it does not address the issue of unintentionally simulating an acoustic cavity equal to the domain size. On the top and bottom boundaries, it is difficult to construct satisfactory conditions unless an algorithm for perfect wave transmission out of the domain is incorporated (for  $\nu > \nu_c$  on the top boundary and for all waves at the bottom boundary). The challenge for such a condition is that it must be general, i.e., able to handle MAG waves in a background flow.

Traditional approaches to remove unphysical wave reflections involve buffering the computational domain with sponge layers in which artificial damping is employed. While small-wavelength modes may be adequately damped, long-wavelength waves, on the order of the computational domain, experience significant reflections. With traditional sponge layers there is no satisfactory way to control the problem since increasing the damping only compounds internal reflections from gradients in the damping layer, and relaxing the damping imposes a requirement to increase the size of the sponge layer and with it the

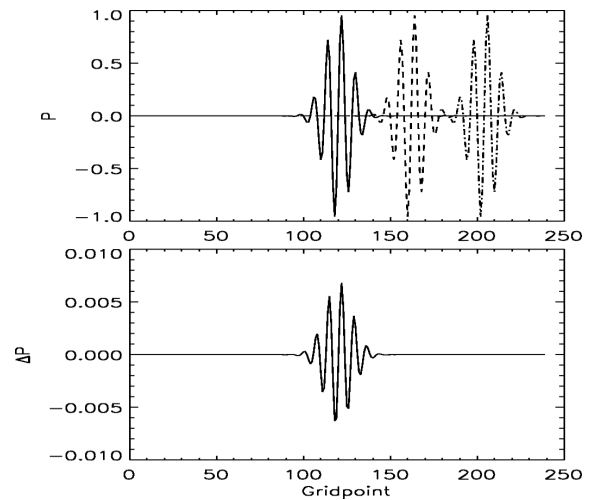


Figure 3. 1-D wave-dispersion tests for the pseudo-spectral algorithm. Top panel shows the evolution of the pressure in a Gaussian wave packet at 0, 140, and 280 time steps. The bottom panel shows the numerical error after 2400 time steps.

computational cost.

We have addressed the problem by developing a new technique based on recent research in acoustic and electromagnetic-wave propagation and reflection called Perfectly Matched Sponge Layers or PML's (Hasthaven 1999, Abarbanel et al. 1999). The technique involves identifying the wave-dispersion relationship desired near boundaries, then adding appropriate time-evolving wave-sink terms to cancel (perfectly) any waves reflected from the interface between the domain interior and the near-boundary damping zone. Unlike traditional sponge layers, this formulation allows specification of very large damping rates which can completely absorb a spectrum of incident waves. Figure 2 demonstrates the procedure for both acoustic and gravity waves and compares the behavior with more conventional sponge-layer methods based on Rayleigh damping and Newton cooling. We note that because the PML method performs so well, the boundary conditions used at the outer most edges of the domain are immaterial, making this procedure compatible with spectral algorithms, whose typically restrictive boundary conditions would be otherwise problematic. We are currently modifying our PML conditions to include the effects of magnetic fields and flows.

### 2.3. Sound sources

The nonlinear processes associated with MAG-wave generation are represented in Equations 1–5 via the terms  $\mathbf{S}$ ,  $S_p$ , and  $\mathbf{S}_b$ . Their forms are deduced from the nonlinear MHD equations. They include a dynamic pressure added to  $p$  in Equation 1 and energy-

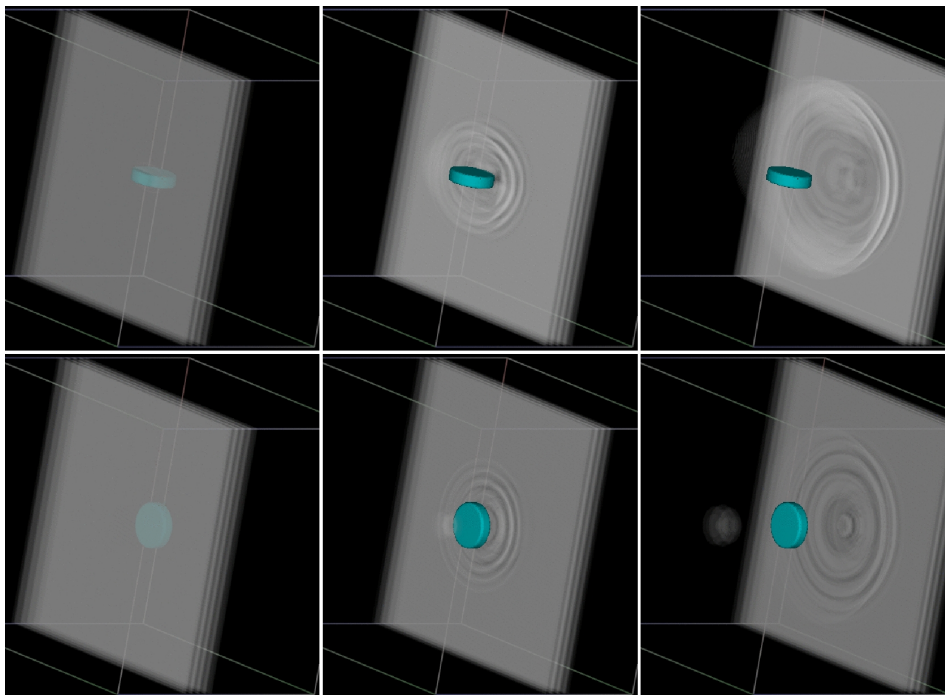


Figure 4. Impact of a Gaussian acoustic wave packet with a coin-shaped sound-speed anomaly; see text.

flux gradients added to Equation 3. The size and distribution of these terms may be estimated from nonlinear simulations (e.g., Nordlund & Stein 2001, Stein et al. 2004). Comparison with SOHO/GOLF observations (Roca Cortes et al. 1999), corrected for the differing mode masses of the Sun and local-area simulations, indicates excellent agreement for the rate of  $p$ -mode stochastic energy input. Hence, the work of Stein et al. (2004), Nordlund & Stein (2001), and Samadi et al. (2003a,b) can be adapted with confidence for specifying the sound-source distribution in linear simulations, allowing us to realize the advantages of the linear wave-propagation approach laid out in §2.1.

## 2.4. Numerical implementation

We have implemented Equations 1–5 using a pseudo-spectral algorithm which is formally  $N$ th-order accurate (where  $N$  is the number of spectral modes used in a given spatial direction, Gottlieb & Orszag 1977). Equation 5 is enforced by decomposing  $\mathbf{b}$  with a two-streamfunction formulation. Field variables are advanced in spectral space with a 3rd-order hybrid implicit/explicit time-stepping scheme (Spalart et al. 1991). Terms containing  $P_0(\mathbf{x}, t)$ ,  $\mathbf{U}_0(\mathbf{x}, t)$ , or  $\mathbf{B}_0(\mathbf{x}, t)$  are treated explicitly, and all other terms are handled implicitly. Field variables are represented by Fourier modes in the horizontal directions and either Fourier or Chebyshev modes in the vertical. Vertical stacking of Chebyshev domains is possible. Other vertical discretizations could also be used. Spatial

derivatives are computed in spectral space. Advection terms are computed efficiently by multiplication in physical space; Fast Fourier Transforms are used to move between the spectral and physical domains.

Tests using this algorithm demonstrate it to be well suited for simulating MAG-wave propagation. Figure 3 shows a test using a unit-amplitude Gaussian wave packet (i.e., a Gabor wavelet) with a carrier wavelength of  $\lambda = 4$  Mm and a FWHM range of  $\Delta\lambda = 18.3$  Mm. The sound speed is set at a uniform constant value of  $c = 36$  km/s. Side boundaries are periodic so that the wave packet may propagate through the box indefinitely. In the top panel the solution is plotted at 0, 140, and 280 time steps. The solution translates uniformly, as expected, with nearly zero dispersion and very little numerical reduction in the wave amplitude. The bottom panel shows the error in the solution after 2400 time steps, during which time the wave packet has propagated nearly 400 Mm and has experienced a reduction in amplitude of only 0.7%. This should be compared to naturally occurring  $p$ -mode damping, which would reduce this wave by a factor of  $4 \times 10^{-6}$  (i.e., by nearly 100%) over the same distance (assuming a damping length of  $\ell_d \approx 30$  Mm). Hence, the numerical error introduced by our computational procedure is effectively zero for realistic solar simulations.

A second demonstration of the performance of the algorithm described above is presented in Figure 4, which shows computed 3-D acoustic-propagation solutions through a sound-speed anomaly. The

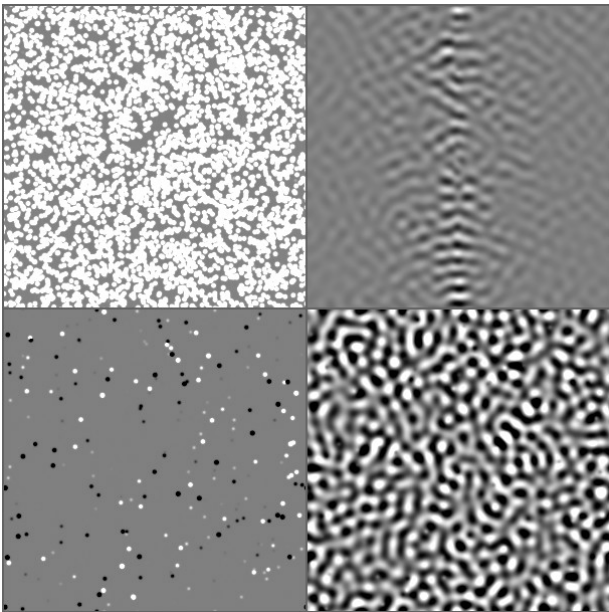


Figure 5. 2-D photospheric simulation results after 512 minutes of time integration. The lower left panel shows a snapshot of the sound sources used with light (dark) areas indicating local expansion (compression). The lower right panel shows the photospheric response via the pressure field. The upper left panel marks the history of the random locations occupied by all of the sources during the simulation. The upper right panel shows a snapshot of the difference in the pressure field between two solutions, one with an embedded flow and one without.

anomaly is a truncated cylindrical disk (shaped somewhat like a thick coin) with a 40 Mm diameter and a 10 Mm thickness. The sound speed inside (outside) the anomaly is 50 km/s (36 km/s). The acoustic wave packet shown in Figure 3 is propagated through the anomaly at two different orientations, and a 3-D volume rendering of the pressure field is shown. The wave refracts and reflects upon encountering the anomaly. In the top row of panels, an asymmetric solution results because of the orientation of the anomaly. In the bottom row, a cylindrically symmetric solution is produced, as the flat surface of the anomaly faces the oncoming wave. Specular backscatter occurs, as is evident from the small reflected wave shown in the middle and right lower panels. Backscatter also occurs in the case depicted in the upper row of panels, but the visualization presented does not show the lower values in the pressure field that result.

The importance of the demonstration shown in Figure 4 is the ability of direct simulation to reproduce physical effects such as backscatter from a sound-speed anomaly. Such effects are not possible when approximate solutions to the wave equation are computed (e.g., the parabolic approximation, see

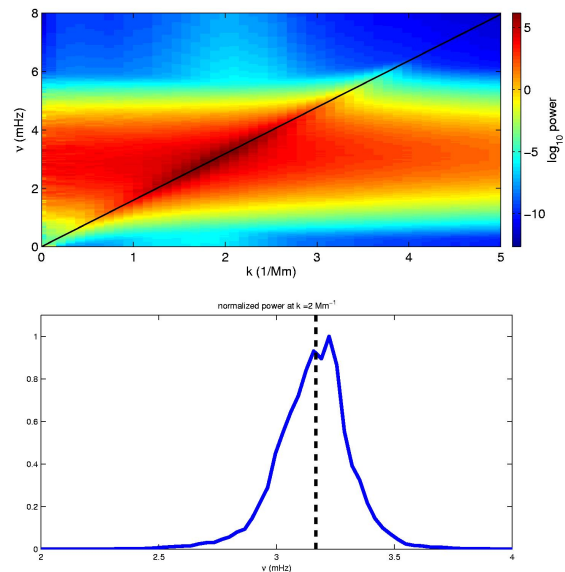


Figure 6. Power spectrum for the artificial data presented in Figure 5. Upper (lower) panel shows the  $k - \nu$  diagram (power versus  $\nu$  at fixed  $k$ ).

Brüggen 2000). As a result, when studying complex wave-damping and -scattering processes, direct simulation will allow us to accurately compute solutions and avoid the need to attempt ad-hoc parameterization of poorly understood processes.

### 3. PHOTOSPHERIC EXAMPLE

As an example of artificial data more relevant to local helioseismology, in this section we present a simple 2-D model of a 60 Mm  $\times$  60 Mm patch of the photosphere which includes specified sound sources and an embedded photospheric flow. In this case the sound sources are included via Equation 1 through  $\mathbf{S}$ , which is constructed to describe a time rate of change for  $\nabla \cdot \mathbf{u}$ . Individual sources possess a Gaussian shape with a (FWHM) diameter of 0.5 Mm and the time dependence of a Gaussian wavelet with a central frequency of  $\nu = 3$  mHz and FWHM frequency range of  $\Delta\nu = 1.5$  mHz (so that the FWHM duration is about 11 minutes). The time and location chosen for each source to instigate excitation are random, with, on average, 90 sources being initiated within any 11 minute time window.

We choose a constant sound speed of  $c = 10$  km/s, producing a dominant acoustic wavelength of  $\lambda = c/\nu = 3.3$  Mm. We also include Newton-cooling via  $S_p = -\eta(p - \rho c^2/\gamma)$ , where  $\eta = 0.0018$  s $^{-1}$  is the damping coefficient required to produce an acoustic damping length of  $\ell_d \approx 30$  Mm. The 0.5 Mm sources and the resulting wave field are resolved with a grid

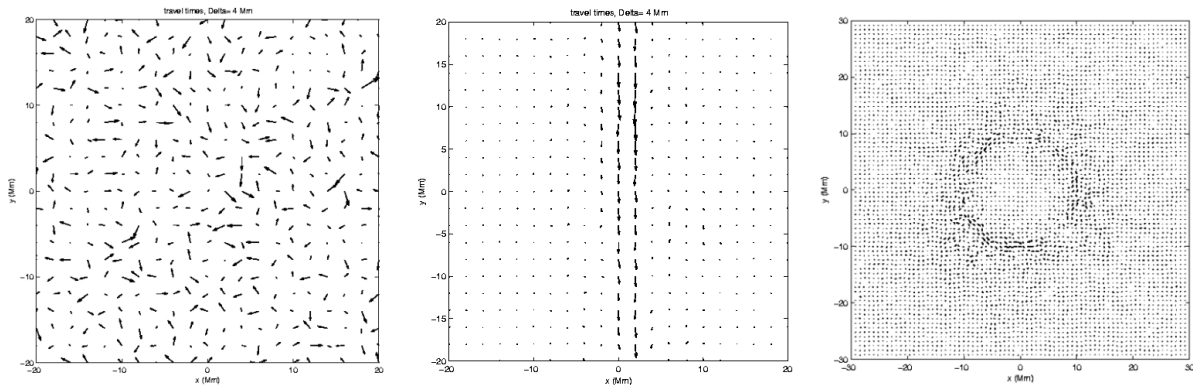


Figure 7. Travel times for artificial data. Left (middle) [right] panel is for sources only (north-south jet) [ring flow]. The maps in the middle and right panels are differences from the case with sources only.

resolution of  $\delta x = 0.2$  Mm. The time step is chosen to be  $\delta t = 10$  s, equivalent to a CFL condition of  $\text{CFL} = c \delta t / \delta x = 0.5$ .

Figure 5 shows results from the simulation after 512 minutes of time integration. The lower left panel depicts a snapshot of the sound sources with light (dark) areas indicating local expansion (compression) by the sources. The lower right panel shows the photospheric response via the pressure field. Animations of this field depict continual fluctuations in response to the blinking sound sources. The upper left panel marks the history of the random locations occupied by all of the sources that have fired during the 512 minute simulation. The upper right panel shows a snapshot of the difference in the pressure field between two solutions, one with an embedded flow and one without. The flow specified is a north-south oriented jet of a raised-cosine form  $U_0 = 0.5A(1 + \cos(ax))$  with amplitude  $A = 1$  km/s and width given by  $a = 2\pi/4$  Mm.

Figure 6 shows the  $k - \nu$  power spectrum of the pressure field for the computed solutions (top panel). A broad band due to the specified forcing is centered at  $\nu = 3$  mHz; note the logarithmic color scale. The expected acoustic resonance response at  $\lambda \nu = c$  is indicated by the solid line. The lower panel shows a slice through the  $k - \nu$  diagram on a linear scale at fixed  $k$ . A resonance peak in the normalized power spectrum is plainly evident with width  $\sim 0.3$  mHz FWHM, consistent with the specified damping rate.

Figure 7 shows results for acoustic travel times computed from cross-correlations of the pressure data, like that depicted in the lower right panel of Figure 5. The cross-correlation is computed for each point in the domain with each of the surrounding quadrants (north, south, east, west) of a 1 Mm (i.e., 1-pixel) wide annulus with inner radius  $\Delta = 4$  Mm.

Travel times are then obtained as described in Gizon & Birch (2004). Figure 7a shows the travel-time map for artificial data computed with sources only; this represents our reference data. Figures 7b and c depict differences in travel-time maps resulting from the reference data and data with embedded flows. The result shown in Figure 7b is for the 4 Mm-wide north-south oriented jet described earlier. Figure 7c shows results for a 4 Mm-wide, 20 Mm-diameter ring flow. A finer resolution output grid is used to present the ring-flow results in an attempt to depict the flow profile in more detail. We note that the relatively high noise in the analyzed results is due to our choice of a single radius for our annulus when computing the travel-time maps.

#### 4. CONCLUSIONS

We have outlined the need for control experiments in local helioseismology. Ambiguous or conflicting results regarding 1) the depth of supergranulation and 2) flows and thermal variations near and beneath sunspots have been reported using different local seismic analysis techniques. Application of these different methods to known synthetic data would help tremendously in evaluating uncertainties associated with the different approaches. In addition, the development of a flexible facility for generating artificial data would allow us to create data sets designed to address specific open questions in local helioseismology. We have presented our preliminary efforts to develop a set of tools for this purpose. They involve solving the linear MHD equations with specified source, radiation, and damping terms for propagating MAG-wave fields. The approach possesses distinct advantages for examining large-scale fields and for devising specific control experiments.

## ACKNOWLEDGMENTS

We appreciate useful and enlightening exchanges with Jesper Jensen, Charlie Lindsey, Doug Braun, and Martin Woodard. This work was supported by NASA contract number NNH04CC05C.

## REFERENCES

- Abarbanel S., Gottlieb D., Hasthaven J.S., 1999, *J. Comp. Phys.*, 154, 266.
- Barnes G., Cally P., 2001, *Astro. Soc. Aus.*, 18, 243.
- Birch A., 2004, The current status of theory for time-distance helioseismology, these proceedings.
- Birch A., Kosovichev A., 2000, *Sol. Phys.*, 192, 193.
- Birch A., Kosovichev A.G., Price G.H., Schlottmann R.B., 2001 *ApJ Let.*, 561, L229.
- Braun D.C., 1995, *ApJ*, 451, 859.
- Braun D.C., 1997, *ApJ*, 487, 447.
- Braun D.C., Lindsey C., 2000, *Sol. Phys.*, 192, 307.
- Braun D.C., Lindsey C., 2003, in *Proc. SOHO 12/GONG+ 2002 Workshop ESA SP-517*, 15.
- Braun D., Birch A., Lindsey C. 2004, *Local Helioseismology of Near-surface Flows*, these proceedings.
- Brüggen M., 2000, *Sol. Phys.*, 192, 225.
- Cally P.S., Bogdan T.J., 1997, *ApJ*, 486, L67.
- Cally P.S., 2000, *Sol. Phys.*, 192, 395.
- Cally P.S., 2004, *Acoustics of Surface Magnetic Fields*, these proceedings.
- Cally P., Crouch A., Braun, 2003, *MNRAS*, 346, 381.
- Canuto C., Hussaini M., Quarteroni A., Zang T., *Spectral Methods in Fluid Dynamics*, Springer Verlag (Berlin and New York), 1988 - second revised printing 1990.
- Christensen-Dalsgaard, et al., 1996, *Sci.*, 272, 1286.
- Christensen-Dalsgaard, 2002, *Rev. Mod. Phys.*, 74, 1073.
- Duvall T.L., Jr., 1998, in *Proc. SOHO 6/GONG 98 Workshop ESA SP-418*, 581.
- Duvall T.L., Jr., D'Silva S., Jefferies S.M., Harvey J.W., Schou J., 1996, *Nature*, 379, 235.
- Fan Y., Braun D., Chou D.-Y., 1995, *ApJ*, 451, 877.
- Gizon L., 2004, statement made at SOHO 14/GONG 2004 workshop, New Haven, CT, USA.
- Gizon L., Birch A.C., 2002, *ApJ*, 571, 966.
- Gizon L., Birch A.C., 2004, *Time-distance Helioseismology: Noise Estimation*, *ApJ*, accepted.
- Gottlieb D., Orszag S.A., 1977, *Numerical Analysis of Spectral Methods: Theory and Applications*, SIAM-CBMS, Philadelphia.
- Gough D.O., Merryfield W.J., Toomre J., 1992, in *GONG 1992, ASP Conf Ser. Vol. 42 ed. T.M. Brown, Astron. Soc. Pac.*, p.257
- Haber D., Hindman B.W., Toomre J., Bogart R.S., Larsen R.M., 2002, *ApJ*, 570, 855.
- Hasthaven J.S., 1999, *J. Comp. Phys.*, 142, 129.
- Jensen J.M., Olsen K.B., Duvall T.L., Jr., Jacobsen B.H., 2003, in *Proc. SOHO 12/GONG+ 2002 Workshop ESA SP-517*, 319.
- Julien K.A., Gough D.O., Toomre J., 1995, in *Proc. of the 4th Ann. SOHO Workshop ESA 2*, 155.
- Kosovichev A.G., Duvall T.L., 1997, In *SCORE'96: Solar Convection and Oscillations and their Relationship*, eds Pijpers, Christensen-Dalsgaard, Rosenthal, Kluwer, Dordrecht, 241.
- Kosovichev A.G., Duvall T.L., Jr., Scherrer, P.H., 2000, *Sol. Phys.*, 192, 159.
- Korzennik S.G., 2001, in *Proc. SOHO 10/GONG 2000 Workshop ESA SP-464*, 149.
- Lindsey C., Braun D.C., 2003, in *Proc. SOHO 12/GONG+ 2002 Workshop ESA SP-517*, 23.
- Lindsey C., Braun D.C., 2004a, *Principles of Seismic Holography for Diagnostics of the Shallow Subphotosphere*, *ApJ*, in press.
- Lindsey C., Braun D.C., 2004b, *The Acoustic Showerglass. I. Seismic Diagnostics of Photospheric Magnetic Fields*, *ApJ*, submitted.
- Lindsey C., Braun D., Jefferies S., Woodard M., Fan Y., Gu Y., Redfield S., 1996, *Apj*, 470, 636.
- Nordlund Å, Stein R.F., 2001, *ApJ*, 546, 576.
- Roca Cortes T., Montanes P., Palle P.L., Perez Hernandez F., Jimenez A., Regula C., and the GOLF Team: 1999, in *Theory and Tests of Convective Energy Transport*, eds A. Gimenez, E. Guinan, B. Montesinos, *ASP Conf. Ser.* 173, 305.
- Rosenthal C.S., Julien K.A., 2000, *ApJ*, 532, 1230.
- Samadi R., Nordlund Å., Stein R.F., Goupil M.J., Roxburgh I., 2003a, *A&A*, 403, 303.
- Samadi R., Nordlund Å., Stein R.F., Goupil M.J., Roxburgh I., 2003b, *A&A*, 404, 1129.
- Skartlien R., 2002, *ApJ*, 565, 1348.
- Spalart P.R., Moser R.D., Rogers M.M., 1991, *J. Comp. Phys.*, 96, 297.
- Stein R., Georgobiani D., Trampedach R., Ludwig H., Nordlund Å, 2004, *Sol. Phys.*, 220, 229.
- Tong C.H., Thompson M.J., Warner M.R., Pain C.C., 2003, *ApJ*, 593, 1242.
- Tong C.H., Thompson M.J., Warner M.R., Rajaguru S.P., Pain C.C., 2003, *ApJ Let.*, 582, L121.
- Woodard M.F., 1997, *ApJ*, 485, 890.
- Zhao J., Kosovichev A.G., 2002, in *Proc. SOHO 12/GONG+ 2002 Workshop ESA SP-517*, 417.
- Zhao J., Kosovichev A.G., 2002, *ApJ*, 591, 446.
- Zhao J., Kosovichev A.G., Duvall T.L., Jr., 2001, *ApJ*, 557, 384.